Chemical reaction mechanisms of solid state ammonia and hydrogen under high pressure

Junyi Miao,[1] Shi He,[1] Kaihua He,[1] Kewei Ding,[2,3,*] Wei Dai,[4] and Cheng Lu[1,†]
[1]*School of Mathematics and Physics, China University of Geosciences (Wuhan), Wuhan 430074, China*
[2]*State Key Laboratory of Fluorine and Nitrogen Chemicals, Xi'an 710065, China*
[3]*Xi'an Modern Chemistry Research Institute, Xi'an 710065, China*
[4]*School of Mathematics and Physics, Jingchu University of Technology, Jingmen 448000, China*

(Received 14 March 2024; revised 17 June 2024; accepted 23 July 2024; published 12 August 2024)

Ammonia is the most stable compound of nitrogen and hydrogen at ambient pressure. However, the chemical reaction of nitrogen and hydrogen is more complex and difficult to explore at high pressures. Here, we have performed extensively structural searches of ammonia-hydrogen compounds based on particle swarm optimization algorithms and first principles calculations. The calculated results show that the main reaction products of nitrogen and hydrogen under high pressure can be divided into two categories: high-energy density material (HEDM) and hydrogen storage material (HSM). Three different phases of NH_4 are potential HEDMs, which are found to be stable or metastable at 40 GPa to 300 GPa, and metastable at ambient pressure with energy density of about 2.15 kJ/g $\sim$ 3.86 kJ/g. The *Pm* phase of NH_{10} is an outstanding HSM with ultrahigh hydrogen storage (41.7 wt%) and release (29.2 wt%) capacities. These findings offer significant insights into the structural arrangements and chemical bonding patterns of ammonia-hydrogen compounds at high pressure, and suggest potential experimental avenues for elucidating how diverse metastable structures with distinct properties might be existed in planetary interiors.

DOI: 10.1103/PhysRevMaterials.8.083604

I. INTRODUCTION

Hydrogen is the most common element in the universe and accounts for up to three-quarters of the total mass of all normal matter [1]. It is a gaseous molecule at ambient conditions [2,3]. Normally, hydrogen is recognized as an ideal energy material due to its high-combustion heat and completely nonpolluting with single-combustion product [4]. In addition, hydrogen is very reactive and can react with almost all elements [5–14]. It plays an important role in both industrial production and modern life. In the past few decades, various hydrogen-rich compounds have been reported, such as the cubic fluorite-type CaH_2 synthesized by Mizoguchi *et al.* [15] via a cationic substitution method with La or Y, which is a potential material for next-generation energy storage devices. Another good example is the electrical-insulated MgH_2 prepared by Stampfer *et al.* [16] at high temperature and high hydrogen pressure conditions, which can be used as a dehydrogenation catalyst in certain chemical reactions, facilitating the removal of hydrogen from other compounds. However, the hydrogen contents of these metal hydrides are relatively low due to the large mass of metal atoms, which hinders their application in efficient hydrogen-storage media. Researchers are conducting studies to enhance the kinetics and thermodynamics of hydrogen release and uptake to make these hydrides more practical for these hydrogen-related applications.

Nitrogen is an abundant element on the Earth. It possesses a relatively light mass, with an atmospheric content of 79% by volume [17]. Its favorable reactivity with hydrogen causes a variety of products, including: hydrazine (N_2H_4) [18], hydrazoic acid (N_3H) [19], diazene (N_2H_2) [20], and ammonia (NH_3) [21]. Extensive theoretical and experimental studies have identified nitrogen hydrides with high hydrogen capacity and high-energy density due to the special chemical bonding patterns and nitrogen backbone chains. Diazene exhibits hydrogen capacity of 6.7 wt%, hydrazine has a high hydrogen capacity of 12.6 wt% and ammonia possesses an even higher hydrogen capacity of 17.6 wt%. Meanwhile, the arrangements of nitrogen atoms exhibit rich diversities. Hydrazine features N–N single bonds in its structure (H_2N–NH_2), while azide ions ($N_3 \rightarrow N^- = N^+ = N^-$) and diazene ($N^- = N^-$) display N = N double bonds. The chemical reactions of these nitrogen hydrides under specific conditions lead to the formation of the N $\equiv$ N triple bonds, releasing a substantial amount of energy due to the significant energy differences between nitrogen and nitrogen chemical bonds (single, double, and triple bonds) [22–25]. These considerable numerical values render them critical HSMs and HEDMs, thereby sparking extensive interest in their synthesis, catalytic decomposition, and physical properties. Among these nitrogen hydrides, ammonia stands out as both a green energy carrier and an alternative fuel [26]. It exists as the sole stable hydronitrogen at ambient conditions, which presents as gaseous molecules with a molecular hydrogen bond, and exhibits an ionic nonhydrogen-bonded feature under high pressure [27,28].

Ammonia and hydrogen are regarded as the predominant constituents within the interior of giant planets Uranus and

*Contact author: dkw204@163.com
†Contact author: lucheng@calypso.cn

Neptune, where conditions of ultrahigh pressure and temperature prevail [29–31]. Despite the absence of direct evidence for reaction between ammonia and hydrogen molecules, there is a prevailing belief that such a reaction may occur under extreme conditions of the interiors of giant planets [32]. Relevant theoretical and experimental studies are expected to reveal the reaction productions and associated processes [33–35]. Thus, the explorations of the physical and chemical properties of hydronitrogens are deemed crucial for understanding of the intricate behaviors within the interiors of giant planets.

In this work, the structural evolutions, electronic properties and hydrogen storage capacities of ammonia-hydrogen compounds under high pressure up to 300 GPa are studied by the widely recognized CALYPSO structure search method in conjunction with first-principles calculations [36–44]. The results indicate that the ammonia hydride of NH_4 undergo the structural phase transition from Pc phase to $P1$ phase at 112 GPa, and then transform to $C2/c$ phase at 190 GPa. These phases display notable energetic, mechanical, and dynamical stabilities under high pressure. Remarkably, all three phases maintain mechanical and dynamical stabilities after decompression to ambient conditions, showing the characteristics of HEDMs. The energetic analyses demonstrate that the $P1$ phase of NH_4 exhibits a high-energy density of 3.86 kJ/g. Moreover, the Pm phase of NH_{10} reveals exceptional hydrogen storage performance with remarkable hydrogen storage capacity of 41.7 wt% and release capacity of 29.2 wt%.

II. THEORETICAL METHODS

The crystal structure searches of ammonia-hydrogen compounds at various pressures (0 GPa, 40 GPa, 100 GPa, 150 GPa, 200 GPa, and 300 GPa) are conducted by using the CALYPSO method and first principles calculations [36,45,46]. Hydronitrogens with various stoichiometries of NH_x ($x = 4$, 5, 6, 7, 10, and 11) at different pressures are searched by the CALYPSO structural prediction method and first-principles calculations. The fixed (1, 2, 4) and variable (1 to 4) unit cell searches are carried out. We perform 50 generations of structural searches with each generation containing 30 structures. The 30% structures are randomly generated, while the rest are generated by a particle swarm optimization algorithm. Based on the criteria, including low energy, high symmetry and structural diversity, 20 low-lying structures are selected from approximately 1500 structures for further high-accuracy re-optimization. Finally, nine stable and metastable structures are obtained, which are shown in Fig. 1. It has been extensively used in various systems [37–44]. Both fixed and variable composition structural searches of ammonia-hydrogen compounds under high pressure are performed. The calculations of total energies, structural relaxations and electronic properties are carried out using the generalized gradient approximation (GGA) with the Perdew-Burke-Ernzerhof (PBE) [47] exchange-correlation functional [48] as implemented in VASP code [49]. The projector-augmented wave method [50] is employed $1s^1$ of H and $2s^2 2p^3$ of N treated as the valence electrons. The kinetic energy cutoff of 550 eV is adopted. Denser k-point sampling is used to ensure the energy convergence. The van der Waals

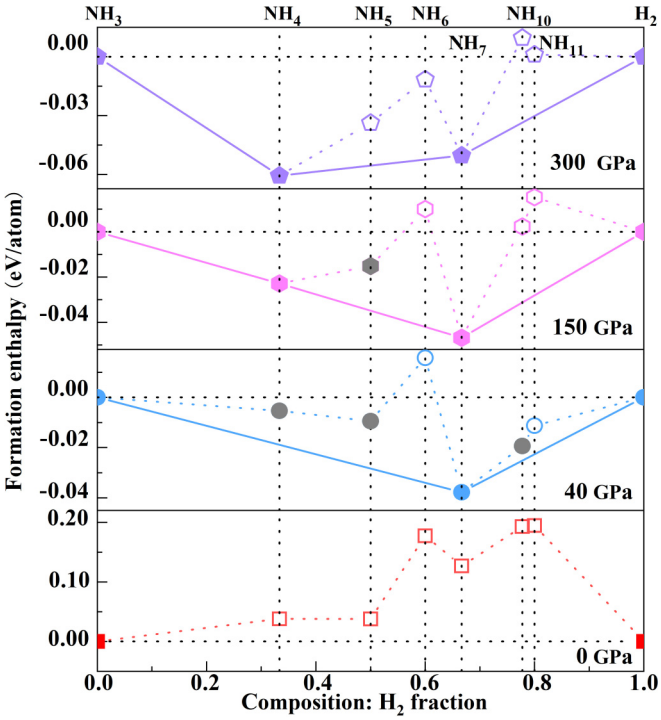

FIG. 1. Formation enthalpies of ammonia-hydrogen compounds relative to solid NH_3 and H_2. The convex hulls (the solid shapes) of the stable phases are connected by the solid lines. Metastable and unstable phases are marked by gray solid shapes and unstable phases are represented by the open shapes, respectively.

(vdW) interactions are also considered by using the DFT-D2 vdW corrections. The energy and force converged in the structural optimizations are set as 1×10^{-6} eV and 1×10^{-4} eV per atom, respectively. The phonon dispersions are calculated by using PHONOPY code [51]. In addition, the zero-point energies (ZPE) are considered and calculated by using the quasi-harmonic approximation.

III. RESULTS AND DISCUSSIONS

We have performed a wide range of structural searches for ammonia-hydrogen compounds at different pressures of 0 GPa, 40 GPa, 100 GPa, 150 GPa, 200 GPa, and 300 GPa. To evaluate the chemical stabilities of NH_x, we calculate their formation enthalpies relative to the elemental solid. We have considered the $P6_3/m$ and $C2/c$ phases of solid hydrogen [52] and the $P2_12_12_1$ and $Pma2$ phases of solid ammonia at the corresponding pressures [53]. The formation enthalpies are defined by the following equation:

$$H_f = \frac{\left[H_{NH_x} - \left(\frac{(x-3)}{2}\right)H_{H_2} - H_{NH_3}\right]}{(x+1)}, \quad (1)$$

where H_f is the formation enthalpy per atom of NH_x compounds, H_{H_2} is the enthalpy of H_2, and H_{NH_3} is the enthalpy of ammonia. The convex hulls, based on the calculated formation enthalpies of each NH_x compound, are shown in Fig. 1, and defined by the solid lines. The solid shapes positioned on the lines represent the thermodynamically stable structures

with the lowest energy of the specific stoichiometries, i.e., the ground states. In comparison, the structures located above the convex hulls are either metastable (solid grey shapes) or unstable (open shapes). As illustrated in Fig. 1 and Fig. S1 in the Supplemental Material (SM) [54], the formation enthalpies of NH_x compounds are greater than 0 eV, indicating that there are no other stable stoichiometries besides ammonia and hydrogen under ambient pressure. Notably, NH_7 is the only stable stoichiometry against decomposition for ammonia-hydrogen compounds below 200 GPa, and is still on the solid lines with pressure increasing to 300 GPa. However, at 300 GPa, NH_4 instead of NH_7 is the most stable ammonia-hydrogen compound.

Here, we first identify that NH_7 is the most stable ammonia-hydrogen compound below 200 GPa, consistent with the findings of Song *et al.* [55] (see Fig. 1 and Fig. S1 [54]), which verifies the accuracy of our current calculations. At ultra-high pressure (300 GPa), the most stable stoichiometry shifts from NH_7 to NH_4; a novel finding in the NH_3–H_2 system. Subsequently, we focus on the metastable compounds (NH_4, NH_5, NH_6, and NH_{10}). Notably, the NH_{10} compound demonstrates a high hydrogen storage capacity (41.7 wt%) and release capacity (29.2 wt%), while NH_4 compounds exhibit favorable detonation properties.

The structural phase transition of NH_7 under high pressure was studied by Song *et al.* [55]. The findings reveal that the hexagonal $R\bar{3}m$ phase of NH_7 at 25 GPa exhibits greater stability compared to the mixture of NH_3 and H_2. With increasing pressure, the $R\bar{3}m$ phase undergoes a structural phase transition at 60 GPa, transforming into the tetragonal $P4_12_12$ phase. Our structure predictions indicate the hexagonal $R\bar{3}m$ phase of NH_7 is an indirect semiconductor with band gap of 3.0 eV. It is stable under 23 GPa and transforms to $P4_12_12$ phase at 65 GPa, which is in good agreement with the previous results reported by Song *et al.* [55], suggesting that the current structure predictions of ammonia-hydrogen compounds under high pressure are reliable. To elucidate the electronic properties of NH_7 under high pressure, we conduct electronic band structure and Bader charge transfer calculations. The corresponding results are illustrated in Figs. S2 and S3 [54] and Table S1 [54]. However, in this work, we mainly focus on the metastable phases of ammonia-hydrogen compounds with distinct structures and properties.

In fact, the metastable phase is also interesting, such as diamond, a metastable phase relative to graphite, which plays an important role in material science [56]. The instability enthalpy ΔH, which quantifies the enthalpy differences between ground state and metastable phase, is a powerful criterion for judging whether the metastable phase can be synthesized [57]. Moreover, more than 80% of the compounds cataloged in the Inorganic Crystal Structure Database (ICSD) are synthesizable with ΔH less than 36 meV/atom [57]. By adopting the threshold instability enthalpy of 36 meV/atom, we have successfully identified four metastable compounds, namely the Pc phase of NH_4, $R3m$ phase of NH_5, $C2/c$ phase of NH_5, and Pm phase of NH_{10}. The respective ΔH values for NH_4, NH_5, and NH_{10} at 40 GPa are: 13.5 meV/atom, 18.9 meV/atom, and 5.8 meV/atom, respectively. Furthermore, the ΔH of NH_5 is determined to be 19.1 meV/atom at 150 GPa.

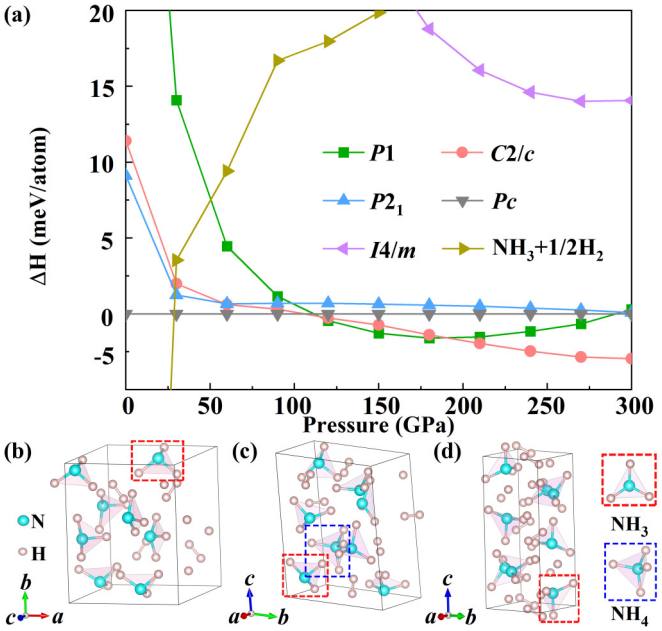

FIG. 2. (a) The calculated enthalpies of various phases of NH_4 with respect to Pc phase at different pressures from 0 GPa to 300 GPa. (b) The Pc phase of NH_4 at 40 GPa, (c) the $P1$ phase of NH_4 at 150 GPa, and (d) the $C2/c$ phase of NH_4 at 300 GPa.

To explore the dynamic stabilities of the aforementioned hydronitrogens, we have calculated the phonon dispersion curves of stable and metastable ammonia-hydrogen compounds. The results are presented in Figs. S4-S9 [54]. No imaginary phonon frequencies are observed in the whole Brillouin zone, confirming the dynamic stabilities of these compounds. We have calculated the mechanical stabilities of these metastable compounds under high pressures (Table S3 [54]). The results show that they are consistent with the mechanical stability criteria [58]. With the increase of pressure, the most stable chemical component of the ammonia-hydrogen compounds changes from NH_7 to NH_4, due to the changes of the hydrogen bonding modes. For instance, at 300 GPa, the $P4_12_12$ phase of NH_7 contains both H_2 moleculars and NH_4^+/H^- ionic units, whereas the $C2/c$ phase of NH_4 is comprised of NH_3 and H_2 molecular units.

It can be seen from Fig. 1 and Fig. S1 [54] that the Pc phase of NH_4 is metastable at 40 GPa and 100 GPa. The NH_3-H_2 system studied by Song *et al.* indicates that NH_4 is thermodynamically stable at pressures above 125 GPa [55]. Our results demonstrate that the $P1$ and $C2/c$ phases of NH_4 are also thermodynamically stable at 150 GPa, 200 GPa, and 300 GPa. In the N-H system investigated by Qian *et al.*, NH_4 is thermodynamically stable within the 50-800 GPa pressure range [59]. Our predicted Pc, $P1$, and $C2/c$ phases of NH_4 are consistent with the results reported by Qian *et al.* [59]. The formation enthalpy calculations for various NH_4 phases relative to NH_3 and H_2 from 0 GPa to 300 GPa are performed with results illustrated in Fig. 2(a). At about 29 GPa, the monoclinic Pc phase of NH_4 becomes more stable than the NH_3 and H_2 mixtures. With the increase of pressure, the Pc phase transforms to a $P1$ phase at 115 GPa, and the $C2/c$ phase of NH_4 becomes the lowest energy structure at 190 GPa

pressure. The Pc phase of NH_4 under low pressure contains 40 atoms (8 formulas) per unit cell with lattice constants of $a = 4.683$ Å, $b = 5.736$ Å, and $c = 5.537$ Å. The structure is composed of NH_3 and H_2 units distributed randomly in the unit cell. The NH_3 units exhibit varying N–H bond lengths ranging from 1.008 Å to 1.032 Å, while H–H distances of H_2 units are 0.732 Å and 0.737 Å. All of the N atoms and H atoms occupied multiple 2a Wyckoff sites. The crystal structure of the Pc phase of NH_4 is shown in Fig. 2(b). Both Pc phase at 40 GPa and $C2/c$ phase at 300 GPa are monoclinic structures with similar structures that contain intriguing NH_3 and H_2 units [Figs. 2(b) and 2(d)]. The triclinic $P1$ phase of NH_4 at 150 GPa exhibits NH_4^+ and H^- units compared to the other two structures, i.e., Pc phase and $C2/c$ phase [Fig. 2(c)]. More structural details are listed in Table S2 [54].

To examine the dynamical stability of NH_4, the phonon band dispersion curves are calculated at 40 GPa, 150 GPa, and 300 GPa. The calculated results are depicted in Figs. S4-S6 [54], which indicate the absence of imaginary frequencies in the entire Brillouin zone. The energy band and density of states (DOSs) are shown in Figs. S10–S12 [54]. The gaps between the valence and conduction bands of the Pc and $P1$ phases of NH_4 are both close to 7.0 eV, which are larger than that of a solid ammonia insulator at 100 GPa (5.3 eV) [59], indicating that they are insulators. By contrast, the energy gap of the $C2/c$ phase is much smaller at 4.9 eV. Meanwhile, the total DOSs are dominated by the N-2p state in both the valence and conduction bands. The orbital hybridizations between N-2p and H-s states indicate the strong N-H covalent interactions in the Pc phase of NH_4. To clearly illustrate the chemical bonding patterns, the electron localization functions (ELF) and Bader charge transfer analyses of NH_4 are performed. As shown in Fig. S13 [54], the strong covalent bonds between the adjacent N and H atoms in NH_4 are identified by the large ELF values. The Bader charge analysis shows that Pc and $C2/c$ phases of NH_4 are molecules characterized by a negligible charge transfer between NH_3 and H_2 units, even at 300 GPa (see Table S1 [54]). However, the $P1$ phase of NH_4 at 150 GPa exhibits both molecular and ionic characters, constituted by the separated H_2 molecules, NH_3 molecules, NH_4^+ ions and H^- ions. Notably, the H_2 and NH_3 molecules exhibit almost no intermolecular charge transfers, indicating their neutral characters. The distinct sizes of NH_4^+ and H^- ions give rise to potential vacancies within the crystal lattice. Ordinarily, such vacancies could induce structural instability; however, the introduced NH_3 and H_2 molecules into these vacancies render the crystal lattice to be stable, particularly under high pressure conditions. These observations also verify the weak interactions between NH_3/H_2 molecules and NH_4^+/H^- ions.

To explore potential HEDMs in ammonia-hydrogen compounds, we decompress the predicted stable and metastable structures of NH_4 from high pressure to ambient pressure. The phonon dispersion curves reveal the dynamical stabilities of the above three phases of NH_4 at ambient pressure, as shown in Fig. 3. The calculated elastic constants of Pc, $P1$, and $C2/c$ of NH_4 at ambient pressure are listed in Table S3 [54], satisfying the mechanical stability criteria [58] of monoclinic and triclinic crystals. It is expected that NH_4 will undergo exothermic decomposition into NH_3 and H_2 at ambient

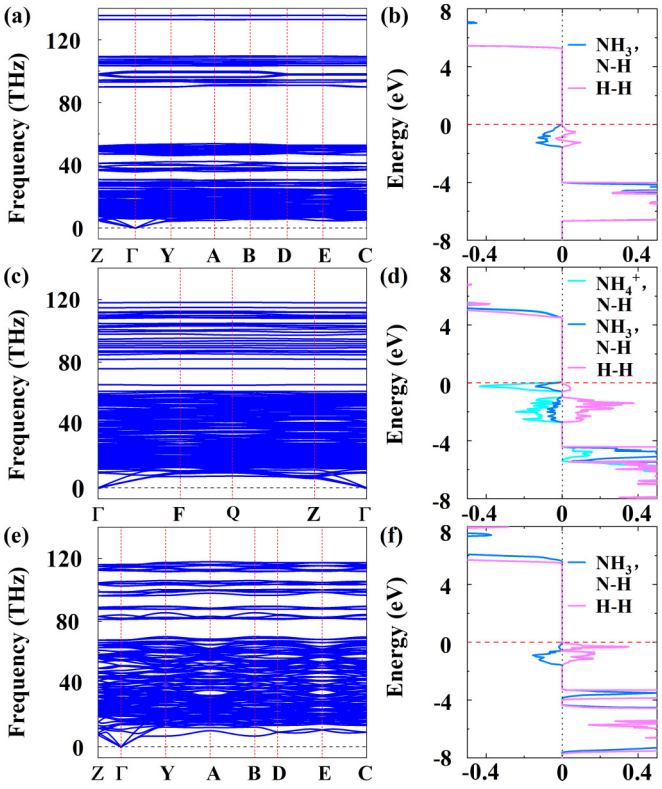

FIG. 3. The phonon dispersion curves and -pCOHPs of NH_4 at ambient pressure. (a) and (b) for Pc phase, (c) and (d) for $P1$ phase, (e) and (f) for $C2/c$ phase.

pressure with the following chemical reactions:

$$NH_4 \longrightarrow NH_3 + 0.5H_2 + ER. \quad (2)$$

Considering the effect of vdW interactions and at the level of zero-point energy (ZPE) corrections based on energy densities, we calculated the chemical energy released during the decomposition of NH_4. The chemical energies released in these reactions are estimated to be 0.44, 0.72 and 0.40 eV for Pc, $P1$, and $C2/c$ phases, with the energy densities of about 2.36 kJ/g, 3.86 kJ/g, and 2.15 kJ/g. The highest energy density is the $P1$ phase of NH_4, which is comparable to TNT [60]. We have conducted calculations for the detonation pressure and detonation velocity of NH_4 compounds in various phases, yielding the following results: $P1$ phase with 39 GPa and 11 km/s, Pc phase with 15 GPa and 8 km/s, and $C2/c$ phase with 25 GPa and 9 km/s. The detonation parameters of the $P1$ and Pc phases of NH_4 compounds exceed those of TNT, while the $C2/c$ phase of the NH_4 compound exhibits comparable detonation pressure and velocity to TNT. In comparison to TNT, the $P1$ phase of NH_4 is a superior HEDM. Its decomposition products are environmentally friendly. As for the same stoichiometric ratio, it is evident that the energy density of NH_4 in the triclinic phase surpasses that of the two monoclinic phases. The energy densities of the two monoclinic phases are more or less the same, which is due to their structural and chemical bonding features. As can be seen from Figs. 2(b)–2(d), the $P1$ phase is characterized as a molecular ionic compound, while the Pc and $C2/c$ phases are identified as molecular compounds. To further explore their

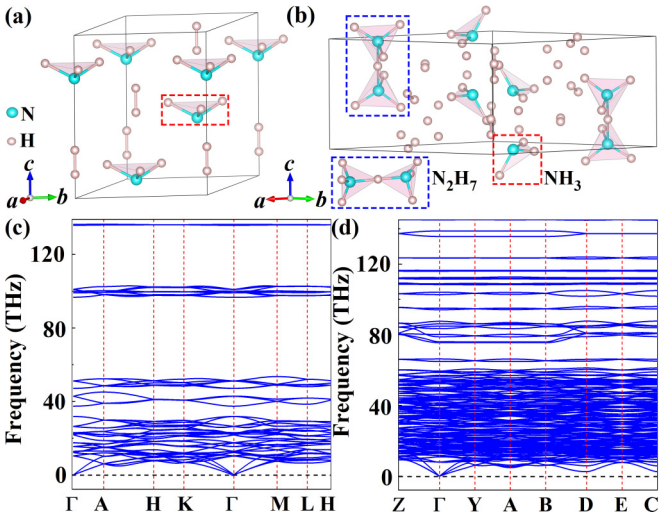

FIG. 4. Crystal structures and phonon dispersion curves of NH_5 compounds. (a) The crystal structure of the $R3m$ phase at 40 GPa. (b) The crystal structure the $C2/c$ phase at 150 GPa. (c) The phonon dispersion curves of the $R3m$ phase at 40 GPa, and (d) the phonon dispersion curves of the $C2/c$ phase at 150 GPa.

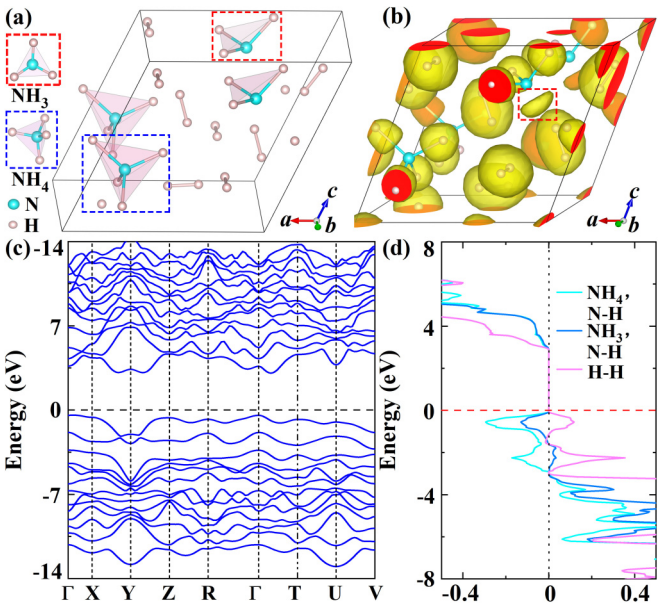

FIG. 5. Crystal structures of the NH_{10} at 40 GPa. (b) ELF of the Pm phase of NH_{10} at 40 GPa. (c) Band structure of the Pm phase of NH_{10} at 40 GPa. (d) The calculated -pCOHP of the Pm phase of NH_{10} at 40 GPa.

chemical bonding behaviors, we have performed the crystal orbital Hamilton population (COHP) calculations [61]. The -pCOHP results are also shown in Fig. 3. A fraction of the N–H bonds within the localized NH_3 units of the three NH_4 phases displays antibonding characteristics. In contrast, the N–H bonds within the localized NH_4 units of the $P1$ phase of NH_4 occupy more extensive regions in the antibonding state, resulting in the increased instability of the crystal lattice, which contributes to the larger enthalpy of the $P1$ phase. Consequently, the greater energy density is observed in the $P1$ phase of NH_4.

NH_5 adopts $R3m$ crystal structure, which is metastable at 40 GPa. It comprises 18 atoms per unit cell. The lattice constants are $a = 3.958$ Å, $b = 3.958$ Å, and $c = 4.913$ Å, respectively. The detailed structural parameters are listed in Table S2 [54]. N atoms occupy the 3a (−0.000, −0.000, 0.735) Wyckoff sites, and H atoms are located at 3a (0.000, 0.000, 0.147), 3a (0.000, −0.000, 0.296), and 9b (0.196, 0.804, 0.484) Wyckoff sites. The crystal structure is depicted in Fig. 4(a). It is constituted by NH_3 and H_2 units. N and H atoms combine to form two distinct units: the tetrahedral-shaped NH_3 units and the separated H_2 units with N–H bond length of 1.022 Å and H–H bond length of 0.730 Å. As the pressure increases, the structure of NH_5 transforms into a monoclinic phase with $C2/c$ symmetry. The crystal structure of $C2/c$ phase of NH_5 at 150 GPa is shown in Fig. 4(b) and the corresponding structural parameters are presented in Table S2 [54]. As shown in Fig. 4(b), the structure of the $C2/c$ phase of NH_5 contains NH_3–H^+–NH_3, NH_3, H_2, and H^- units. It is worth mentioning that the interesting NH_3–H^+–NH_3 ionic units are rare in bulk crystals. The chemical bonds of N–H^+–N in NH_3–H^+–NH_3 ionic units of $C2/c$ phase of NH_5 are not in a straight line with an angle of 178°. Moreover, not all of the NH_3 units in the $C2/c$ phase of NH_5 form the NH_3–H^+–NH_3 ionic units. The rest of NH_3 and H_2 units surround the NH_3–H^+–NH_3 ionic units and form different N–H bonds with distances ranging from 0.98 to 1.19 Å. The interstitial H–H bond length is 0.75 Å.

A comparison of the structural configurations between the two phases of NH_5 reveals a notable increase in the proton-accepting capabilities of the NH_3 units under high pressure. This enhancement serves as a pivotal factor driving the observed phase transition of NH_5 under high pressure, keeping with the findings previously reported by Song *et al.* [55]. Upon probe, the electronic properties of NH_5, the energy band, electronic density of states (DOS), and ELF are calculated and the results are displayed in Figs. S14-S16 [54]. As shown in Figs. S14 and S15 [54], two phases of NH_5 are semiconductors. The band gap of the $R3m$ phase of NH_5 at 40 GPa is 3.9 eV. It is a typical indirect semiconductor. At 150 GPa, the $C2/c$ phase of NH_5 exhibits a band gap of 4.0 eV. The top of the valence band and the bottom of the conduction band align at the Gamma point, indicating that it transforms to a direct semiconductor. The ELF shows the evolution of the chemical bonding patterns of NH_5 under high pressure. With increasing pressure, part of the H_2 molecules begin to decompose and two NH_3 units bind to the decomposed H^+ ions to form the NH_3–H^+–NH_3 ionic units. In fact, the formation of the ionic bonds between NH_3–H^+–NH_3 and H^- units can also be confirmed by the obvious charge transfers between H^+ and H^- ions, as shown in Table S1 [54].

NH_{10} is thermodynamically unstable in the convex hull of ammonia hydrides at 40 GPa, however, the instability enthalpy ΔH is just 5.8 meV/atom, which is much smaller than threshold of 36 meV/atom [57], and thus it is experimentally possible to be synthesized under specific conditions. The crystal structure of NH_{10} at 40 GPa is Pm symmetry, as shown in Fig. 5(a). It contains 22 atoms per unit cell, including the NH_4^+, NH_3, H_2, and H^- units. The lattice constants are $a = 4.899$ Å, $b = 3.513$ Å, and $c = 4.836$ Å, respectively. The N

atoms are located at the 1a Wyckoff sites, while the H atoms are distributed across various 1b and 2c Wyckoff sites. The bond lengths of N–H bonds are about 1.010 to 1.107 Å, and the H–H bond lengths are from 0.736 to 0.754 Å. Detailed structural parameters are displayed in Table S2 [54]. The phonon dispersion curves Fig. S9 [54] show that the *Pm* phase of NH_{10} exhibits an ultra-high hydrogen storage capacity, reaching 41.7 wt%. Additionally, 29.2 wt% of H_2 can be extracted during its decomposition. The remarkable hydrogen storage and release capabilities of the *Pm* phase of NH_{10}, suggest it is a promising hydrogen storage material.

To elucidate the electronic properties of NH_{10}, we calculate the electronic band structures and DOS. The results are presented in Fig. 5(c). There are no bands across the Fermi level. Thus, the *Pm* phase of NH_{10} is a semiconductor with band gap of 3.5 eV. In contrast to other hydrogen-rich structures, both the valence band and conduction band regions exhibit dominance of the hydrogen-s state in the total density of states (TDOS). The strong hybridization effects between N-2*p* and H-*s* states indicate N atoms play the pivotal role in stabilizing the *Pm* phase of NH_{10}. Additionally, the -pCOHP [Fig. 5(d)] analyses show that there are bonding states and a few antibonding states between the N–H pairs. The existence of antibonding states within the molecular framework may induce the structural instability; however, this destabilizing effect is counteracted by the presence of the bonding states within H–H pairs, thereby resulting in the ultimate stabilization of NH_{10}. The interatomic crystal orbital Hamilton population (ICOHP) values for N–H and H–H bonds are −8.32 eV and −6.70 eV, respectively, indicating the stronger N–H interactions in comparison to the H–H interactions. The ELF pattern of NH_{10} is shown in Fig. 5(b). The large ELF values are found between the adjacent N and H atoms, indicating the strong N–H covalent bonds. The Bader charge analyses (see Table S1 [54]) of NH_{10} demonstrate that NH_4^+ ions and NH_3 molecules transfer 0.45 *e* to H_2 molecules and H^- ions, but the H_2 molecules receive very little charge from the NH_4^+ ions, and therefore the H_2 units display as almost neutral, which is in good agreement with the ELF results.

IV. CONCLUSIONS

In summary, we have conducted a comprehensive study of ammonia-hydrogen compounds at high pressure, employing a combination of the CALYPSO method and first-principles calculations. Three stable or metastable high pressure phases of NH_4 are uncovered at high pressure with notable energy densities ranging from approximately 2.15 kJ/g ∼ 3.86 kJ/g upon decompression to ambient pressure. Most importantly, the *Pm* phase of NH_{10} displays an ultra-high hydrogen storage capacity, attaining 41.7 wt%. Furthermore, during its decomposition, a substantial 29.2 wt% of H_2 can be extracted. The outstanding hydrogen storage and release characteristics of NH_{10} suggest it is a promising material for hydrogen storage applications. These findings furnish valuable insights into the structures and chemical bonding patterns of ammonia-hydrogen compounds under high pressure, which may also offer important information to explore the existence of diverse metastable structures with distinct properties in planetary interiors.

ACKNOWLEDGMENTS

This work is supported by National Natural Science Foundation of China under Grants No. 12174352 and No. 12111530103, and the Fundamental Research Funds for the Central Universities, China University of Geosciences (Wuhan) (Grant No. G1323523065).

[1] E. D. Young, A. Shahar, and H. E. Schlichting, Nature (London) **616**, 306 (2023).
[2] M. E. Kilic and K. R. Lee, Phys. Rev. Appl. **18**, 014066 (2022).
[3] E. Gregoryanz, C. Ji, P. D. Simpson, B. Li, R. T. Howie, and H. K. Mao, Matter Radiat. Extremes **5**, 038101 (2020).
[4] R. D. Cortright, R. Davda, and J. A. Dumesic, Nature (London) **418**, 964 (2002).
[5] M. Kandasamy, A. Seetharaman, B. Chakraborty, I. M. Babu, J. J. William, G. Muralidharan, K. Jothivenkatachalam, and D. Sivasubramanian, Phys. Rev. Appl. **14**, 024067 (2020).
[6] J. Shi, W. Cui, J. Hao, M. Xu, X. Wang, and Y. Li, Nat. Commun. **11**, 3164 (2020).
[7] M. S. Somayazulu, L. W. Finger, R. J. Hemley, and H. K. Mao, Science **271**, 1400 (1996).
[8] W. Grochala and P. P. Edwards, Chem. Rev. **104**, 1283 (2004).
[9] M. Somayazulu, P. Dera, A. F. Goncharov, S. A. Gramsch, P. Liermann, W. G. Yang, Z. X. Liu, H. K. Mao, and R. J. Hemley, Nat. Chem. **2**, 50 (2010).
[10] D. K. Spaulding, G. Weck, P. Loubeyre, F. Datchi, P. Dumas, and M. Hanfland, Nat. Commun. **5**, 5739 (2014).
[11] P. Zhang, J. Shi, W. Cui, C. Liu, S. Ding, K. Yang, J. Hao, and Y. Li, Phys. Rev. B **105**, 214109 (2022).
[12] Y. Liang, X. Cui, F. Li, C. Stampfl, S. P. Ringer, J. Huang, and R. Zheng, Phys. Rev. Appl. **18**, 034084 (2022).
[13] U. Ranieri, L. J. Conway, M.-E. Donnelly, H. Hu, M. Wang, P. Dalladay-Simpson, M. Peña-Alvarez, E. Gregoryanz, A. Hermann, and R. T. Howie, Phys. Rev. Lett. **128**, 215702 (2022).
[14] S. Y. Fu, S. Chariton, V. B. Prakapenka, and S. H. Shim, Nature (London) **615**, 646 (2023).
[15] H. Mizoguchi, S. Park, T. Honda, K. Ikeda, T. Otomo, and H. Hosono, J. Am. Chem. Soc. **139**, 11317 (2017).
[16] P. Vajeeston, P. Ravindran, B. C. Hauback, H. Fjellvåg, A. Kjekshus, S. Furuseth, and M. Hanfland, Phys. Rev. B **73**, 224102 (2006).
[17] R. Manjunatha, A. Karajić, V. Goldstein, and A. Schechter, ACS Appl. Mater. Interfaces **11**, 7981 (2019).
[18] R. L. Collin and W. N. Lipscomb, Acta Cryst. **4**, 10 (1951).
[19] G. C. Pimentel, S. W. Charles, and K. Rosengren, J. Chem. Phys. **44**, 3029 (1966).
[20] N. Wiberg, H. Bachhuber, and G. Fischer, Angew. Chem. Int. Ed. Engl. **11**, 829 (1972).
[21] J. W. Erisman, M. A. Sutton, J. Galloway, Z. Klimont, and W. Winiwarter, Nat. Geosci. **1**, 636 (2008).
[22] M. L. Xu, Y. W. Li, and Y. M. Ma, Chem. Sci. **13**, 329 (2022).

[23] L. L. Liu, D. H. Wang, S. T. Zhang, and H. J. Zhang, J. Mater. Chem. A **9**, 16751 (2021).

[24] K. Yang, J. Shi, W. Cui, J. Hao, and Y. Li, Phys. Chem. Chem. Phys. **25**, 20281 (2023).

[25] Y. Li, J. Hao, H. Liu, S. Lu, and J. S. Tse, Phys. Rev. Lett. **115**, 105502 (2015).

[26] Y. C. Wan, J. C. Xu, and R. T. Lv, Mater. Today **27**, 69 (2019).

[27] T. Palasyuk, I. Troyan, M. Eremets, V. Drozd, S. Medvedev, P. Z. Ejgierd, E. M. Palasyuk, H. Wang, S. A. Bonev, D. Dudenko *et al.*, Nat. Commun. **5**, 3460 (2014).

[28] S. Ninet, F. Datchi, P. Dumas, M. Mezouar, G. Garbarino, A. Mafety, C. J. Pickard, R. J. Needs, and A. M. Saitta, Phys. Rev. B **89**, 174103 (2014).

[29] W. B. Hubbard, W. Nellis, A. C. Mitchell, N. C. Holmes, S. S. Limaye, and P. C. McCandless, Science **253**, 648 (1991).

[30] R. Chau, S. Hamel, and W. J. Nellis, Nat. Commun. **2**, 203 (2011).

[31] R. Helled and J. J. Fortney, Philos. Trans. R. Soc. A **378**, 20190474 (2020).

[32] G. M. Borstad and C. S. Yoo, J. Phys.: Conf. Ser. **500**, 032002 (2014).

[33] A. G. Hu and F. Zhang, AIP Conf. Proc. **1426**, 1417 (2012).

[34] A. Karahodza, K. J. Knaus, and D. W. Ball, J. Mol. Struct. (THEOCHEM) **732**, 47 (2005).

[35] L. C. Li, J. Shang, J. L. Liu, X. Wang, and N. B. Wong, J. Mol. Struct. (THEOCHEM) **807**, 207 (2007).

[36] Y. C. Wang, J. Lv, L. Zhu, and Y. M. Ma, Comput. Phys. Commun. **183**, 2063 (2012).

[37] Y. C. Wang, J. Lv, L. Zhu, and Y. M. Ma, Phys. Rev. B **82**, 094116 (2010).

[38] Q. Z. Duan, J. Y. Shen, X. Zhong, H. Y. Lu, and C. Lu, Phys. Rev. B **105**, 214503 (2022).

[39] J. Gou, B. Xia, H. Li, X. Wang, L. Kong, P. Cheng, H. Li, W. Zhang, T. Qian, H. Ding *et al.*, Phys. Rev. Lett. **121**, 126801 (2018).

[40] W. G. Sun, B. L. Chen, X. F. Li, F. Peng, A. Hermann, and C. Lu, Phys. Rev. B **107**, 214511 (2023).

[41] F. Peng, Y. Sun, C. J. Pickard, R. J. Needs, Q. Wu, and Y. Ma, Phys. Rev. Lett. **119**, 107001 (2017).

[42] C. Lu, C. Y. Cui, J. N. Zuo, H. X. Zhong, S. He, W. Dai, and X. Zhong, Phys. Rev. B **108**, 205427 (2023).

[43] C. Lu, W. G. Gong, Q. Li, and C. F. Chen, J. Phys. Chem. Lett. **11**, 9165 (2020).

[44] J. Y. Miao, Z. S. Lu, F. Peng, and C. Lu, Chin. Phys. Lett. **38**, 066201 (2021).

[45] X. Shao, J. Lv, P. Liu, S. Shao, P. Gao, H. Liu, Y. Wang, and Y. Ma, J. Chem. Phys. **156**, 014105 (2022).

[46] S. Liu, W. Lu, X. Zhang, J. Song, J. Lü, X. Liu, Y. Wang, C. Chen, and Y. Ma, Sci. Bull. **68**, 1456 (2023).

[47] J. P. Perdew, K. Burke, and M. Ernzerhof, Phys. Rev. Lett. **77**, 3865 (1996).

[48] J. P. Perdew, J. A. Chevary, S. H. Vosko, K. A. Jackson, M. R. Pederson, D. J. Singh, and C. Fiolhais, Phys. Rev. B **46**, 6671 (1992).

[49] G. Kresse and J. Furthmüller, Phys. Rev. B **54**, 11169 (1996).

[50] P. E. Blöchl, Phys. Rev. B **50**, 17953 (1994).

[51] A. Togo, F. Oba, and I. Tanaka, Phys. Rev. B **78**, 134106 (2008).

[52] C. J. Pickard and R. J. Needs, Nat. Phys. **3**, 473 (2007).

[53] C. J. Pickard and R. J. Needs, Nat. Mater. **7**, 775 (2008).

[54] See Supplemental Material at http://link.aps.org/supplemental/10.1103/PhysRevMaterials.8.083604 for the structural, mechanical, and electronic properties of ammonia-hydrogen compounds at different pressures.

[55] X. Q. Song, K. T. Yin, Y. C. Wang, A. Hermann, H. Y. Liu, J. Lv, Q. Li, C. F. Chen, and Y. M. Ma, J. Phys. Chem. Lett. **10**, 2761 (2019).

[56] R. C. DeVries, Annu. Rev. Mater. Sci. **17**, 161 (1987).

[57] Y. B. Wu, P. Lazic, G. Hautier, K. Persson, and G. Ceder, Energy Environ. Sci. **6**, 157 (2013).

[58] Z. J. Wu, E. J. Zhao, H. P. Xiang, X. f. Hao, X. J. Liu, and J. Meng, Phys. Rev. B **76**, 054115 (2007).

[59] G. R. Qian, H. Y. Niu, C. H. Hu, A. R. Oganov, Q. F. Zeng, and H. Y. Zhou, Sci. Rep. **6**, 25947 (2016).

[60] A. A. Korkin and R. J. Bartlett, J. Am. Chem. Soc. **118**, 12244 (1996).

[61] R. Dronskowski and P. E. Blöchl, J. Phys. Chem. **97**, 8617 (1993).